A general methodology for extracting and categorising flow patterns in turbulent stirred tank mixers based on 2-D network-of-zones (NoZ) model

DOI:
10.1016/j.cherd.2023.05.022

Document Version
Accepted author manuscript

Graphical Abstract

A general methodology for extracting and categorising flow patterns in turbulent stirred tank mixers based on 2-D network-of-zones (NoZ) model

Yuqi Bai, Cláudio Pereira da Fonte, Adam Kowalski, Waldo Rosales Trujillo, Thomas Lawrence Rodgers

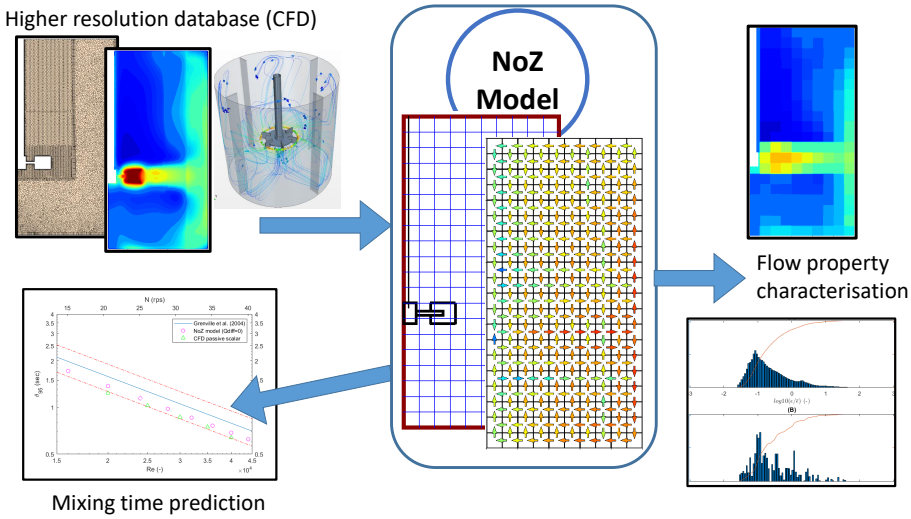

Highlights

A general methodology for extracting and categorising flow patterns in turbulent stirred tank mixers based on 2-D network-of-zones (NoZ) model

Yuqi Bai, Cláudio Pereira da Fonte, Adam Kowalski, Waldo Rosales Trujillo, Thomas Lawrence Rodgers

- Generalised process for coarse-graining flow patterns in stirred tank mixers using network-of-zones model.
- Mixing time estimation based on extracted flow patterns.
- Case studies on two representative radial and axial flow impellers.

A general methodology for extracting and categorising flow patterns in turbulent stirred tank mixers based on 2-D network-of-zones (NoZ) model

Yuqi Bai[a], Cláudio Pereira da Fonte[a], Adam Kowalski[b], Waldo Rosales Trujillo[b], Thomas Lawrence Rodgers[a]

[a] *University of Manchester, Oxford Rd, Manchester, M13 9PL, England, United Kingdom*
[b] *Unilever R&D Port Sunlight Laboratory, Quarry Road East, Bebington, CH63 3JW, England, United Kingdom*

Abstract

A general methodology for characterising stirred tank mixers using two-dimensional network-of-zones (2-D NoZ) model was introduced in this work. Starting from high resolution 3-D velocity field database such as CFD simulations, flow patterns were preserved and simplified into 2-D inter-zonal flowrates and mass imbalances were corrected in the defined routine. Mixing time estimation and turbulent dissipation rate profiles were chosen as metrics for evaluation of the generated 2-D NoZ model, which were compared to CFD passive scalar and literature results on two typical stirred tank geometries covering both radial flow and axial flow impellers.

Keywords: Turbulent mixing, Stirred tank mixers, Flow pattern characterization, Mixing time prediction, Network-of-zones model

Nomenclature

2-D	Two-Dimensional
3-D	Three-Dimensional
ΔR	width of each zone in radial direction, m
ΔZ	height of each zone in axial direction, m
δ_+, δ_-	indicator functions of inflow / outflow

$\|R\|$ normalised mass balance residual, (-)

$\mathbb{CELLS}^m$ set of higher resolution data cells, with a size of m

$\overline{\Gamma}$ mean turbulent diffusion coefficient, $m^2 * s^{-1}$

$\overline{\nu_T}$ mean turbulent kinematic viscosity, $m^2 s^{-1}$

k subscript for arbitrary zone / point

θ angular coordinates, (-)

θ_{95} 95% homogeneity mixing time, sec

C zonal concentration, $kg * m^{-3}$

C_0 initial concentration, $kg * m^{-3}$

C_∞ infinite time concentration, $kg * m^{-3}$

$C_{i,j}$ concentration in $zone(i,j)$, $kg * m^{-3}$

$E^{i,j}$ index notation of the (i+1,j+1)th element in matrix $\mathbf{E}$

H liquid height, m

i, j zone indexes, $0 \leq i \leq R_{div} - 1$,$0 \leq j \leq Z_{div} - 1$

k turbulent kinetic energy, $m^2 s^{-1}$

L, R, B, U Subscript for Left / Right / Bottom / Upper neighbours of the zone

N, N_1, N_2 impeller speed(s), rps

Q inter-zonal flowrates, $m^3 * s^{-1}$

q minor correction flowrates, $m^3 * s^{-1}$

Q_r, Q_z flowrates in radial / axial direction,$m^3 * s^{-1}$

$Q_r^{i,j}$ index notation of the (i+1,j+1)th element in matrix $\mathbf{Q_r}$

$Q_z^{i,j}$ index notation of the (i+1,j+1)th element in matrix $\mathbf{Q_z}$

Q_{diff} global auxiliary inter-zonal flowrate, $m^3 * s^{-1}$

Q_{in}, Q_{out} total flowrates flowing into / out from the zone, $m^3 * s^{-1}$

r, z cylindrical coordinates, m

R mass balance residual, $m^3 s^-1$

R_{div} number of zones in NoZ grid in radial direction (-)

T tank diameter, m

V volume of the zone, m^3

$V^{i,j}$ index notation of the (i+1,j+1)th element in matrix $\mathbf{V}$

v_r radial velocity, $m * s^{-1}$

v_z axial velocity, $m * s^{-1}$

x, y, z Cartesian coordinates, m

Z_{div} number of zones in NoZ grid in axial direction (-)

$zone(i, j)$ the ith in radial and jth in axial zone in NoZ grid

B baffle width, m

C impeller clearance, m

CFD Computational Fluid Dynamics

csv comma-separated values

D impeller diameter, m

LHS Left Hand Side

MRF Multiple Reference Frame

NoZ Network-of-Zones

PBTD Downflow Pitched-Blade Turbine

PC Personal Computer

PIV	Particle Image Velocimetry
RAM	Random-access Memory
Re	impeller Reynolds number, (-)
RHS	Right Hand Side
SKE	Standard K-Epsilon

1. Introduction

Reliable models for the simulation of mixing vessels are important for the understanding of real-life mixing problems. These mixing problems can include a wide range of mixing devices, especially stirred tanks with various impellers and baffle geometries. The mixing performance of industrial mixers with standard geometries have been widely studied both experimentally (Kresta and Wood, 1993; Grenville and Nienow, 2004; Bakker et al., 1996; Jaworski et al., 2001) and computationally (Jaworski et al., 2001; Han et al., 2007; Aubin et al., 2004; Coroneo et al., 2011). Novel non-standard industrial mixers can be evaluated by CFD simulation to see whether the mixer could accomplish the desired mixing task before they are manufactured. For many mixing systems, multi-phase processes complicate the determination of performance, for example gas-liquid mixing, solid-liquid mixing, emulsification, and crystallisation. For all of these systems, flow patterns are important to the mixing performance.

The methodology of zonal modelling (or compartment modelling) in solving differential control equations has been widely adapted in simulating chemical engineering processes, especially on complex reaction systems (Hsu et al., 1994; Vlaev et al., 2000; Komrakova et al., 2017; Jourdan et al., 2019), crystallisation processes (Massmann et al., 2020), biochemical processes (Pigou and Morchain, 2015; Nørregaard et al., 2019; Le Moullec et al., 2010) and precipitation processes (Kagoshima and Mann, 2006). The common feature of these examples of zonal models is that the whole fluid domain is divided into a number of connected fluid "zones", so that in each of the zones the control equations can be simplified by approximations or external experimental data. By this method the time consumption in solving the control equations can be significantly reduced compared to solving on a completely discretised grid via CFD. The number and shape of the fluid zones varies with the literature, the criteria of creating zones, however, can be categorised into two main methods: creating zones by properties and creating zones on geometries. The first method of creating zones is to define a tolerance on one (or a group of) specified property(s), e.g. turbulent dissipation rates, so that all connected fluid elements with the specified fluid property within the tolerance can be considered as one zone (Jourdan et al., 2019; Haag et al., 2018; Bezzo et al., 2003, 2004; Bezzo and Macchietto, 2004; Komrakova et al., 2017; Tajsoleiman et al., 2019; Nauha et al., 2018). This method preserves the volumetric distribution of the key property since all fluid elements in each zone

are physically analogous at least in the aspect of the specified fluid property. Zones generated in this way are usually of irregular shapes, and the number of zones are usually small (typically around or less than 10) (Haag et al., 2018).

The second method of creating zones is to create a geometrical structured grid of zones manually (Kagoshima and Mann, 2006; Rodgers et al., 2011; Hsu et al., 1994; Vlaev et al., 2000). Each zone is regularly shaped and inter-zonal boundaries are orthogonal. This method is typically named as the network-of-zones (NoZ) model. This method usually requires a larger number of zones and generally preserves the spatial distribution of the system and matches the flow patterns in specific geometries. Topology among zones is usually tuned with sub-scale minor flows at specific locations to better describe minor swirls that will enhance mixing, basing on additional knowledge of the studied geometry.

Massmann et al. (2020) studied the semi-batch crystallisation processes by integrating 3-D CFD of a stirred tank crystalliser into a two-dimensional zonal model, combining the concepts of both methods mentioned above. The zones were manually specified with structured zone grid but with small number of zones (up to 9), and inter-zonal flowrates were simplified without adding sub-scale minor flows. An algorithm to reduce mass imbalance errors brought by integrating and interpolating within each zone were also introduced based on minimisation algorithms.

Emulsification is an important process during the production of various goods such as mayonnaise and salad creams in food industries. One major modelling approach for emulsification is the population balance model (Janssen and Hoogland, 2014; Håkansson et al., 2016), which provides a prediction of the entire distribution of droplet sizes between the maximum and minimum droplet size of the dispersed phase via solving a system of 4-10 equations, including the mass conservation equation of dispersed phase in integrated form and a statistical modelling of daughter size distributions (Lebaz and Sheibat-Othman, 2019; Chen et al., 2019). Due to the number of equations to solve and the coupling with turbulent transport equations, the population balance is usually computational expensive on a finely discretised fluid domain, such as CFD mesh grid. This represents an example of a category of challenging systems to model in process industries, where the mainstream flow patterns are important but time consumption for numerical simulation directly via CFD is overly long before plausible decisions for design need to be made in industrial practice.

The purpose of this work is to establish a generalised process for generating a simple 2-D network-of-zones models for an arbitrary stirred tank mixer, so that the flow patterns, mixing time, and energy dissipation distribution could be preserved while simplifying inter-zonal topology. This will allow complex multi-phase systems of equations, e.g. crystal growth or emulsion break-up, to be simultaneously calculated without the computational expense of CFD. A CFD simulation is used as the base for generating the 2-D network-of-zones model, allowing flow rates to be calculated. A mass imbalance remediation algorithm was also built without using minimisation algorithms (different from Massmann et al. (2020)) so as to ensure it did not change core flow patterns and to be more computational-efficient on larger numbers of zones. Mixing time estimation was selected to be a metric to evaluate the performance of this process as well as comparison of the distribution of the energy dissipation rates.

2. Methodology

2.1. Inputs, Specifications, and Outputs

The inputs of the NoZ model were a database containing Eulerian radial (v_r) and axial (v_z) velocities at different 3-D Cartesian coordinates all over the whole tank, with a relatively higher resolution compared to the geometrical scale of the specified zones in specifications. In this work, despite the resolution were redundantly higher than required, all the data used as an input database was exported from converged CFD solutions of each of the tank and impeller geometries. It should be mentioned that the inputs of the methodology does not necessarily need to be from CFD solutions; instead, a 3-D PIV of high enough resolution could also be valid inputs. The tangential velocities were not used as the 2-D NoZ model were only conserving topology in radial and axial direction between adjacent zones. In mathematical form, the database could be represented as a set $\mathbb{CELLS}^m = \{c_1, c_2, c_3, ..., c_m\}$ with m discretised fluid cells which could be represented as a collection of coordinates, velocity components, cell volume V and optional other scalar properties (e.g. turbulent dissipation rates) of fluid as defined in Equation 1:

$$c = \{r, \theta, z, v_r, v_z, V, ...\} \tag{1}$$

The specifications of a NoZ model were the numbers of divisions in both radial and axial direction of the axisymmetric stirred tank, denoted as R_{div}

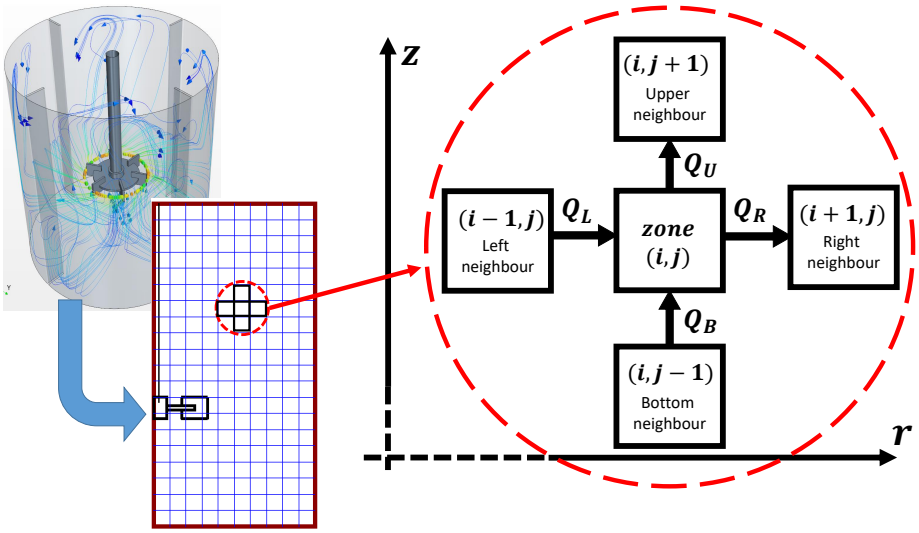

Figure 1: Schematics of the NoZ model, zonal neighbourhood relations and bulk inter-zonal flowrates

and Z_{div} respectively. The value of R_{div} and Z_{div} depends on the size and aspect ratio of the vessel: in general, the impeller should intersect at least four zones so that the zones were not overly large, whilst the aspect ratio of each zone should be close to one. Starting from the symmetry axis and the bottom of the tank where $r = 0, z = 0$ and towards the top edge of the tank where $r = T/2, z = H$, a structured discretisation of the half-tank domain was formed as $R_{div} * Z_{div}$ subdomains. The width of every subdomain was $\Delta R = T/(2R_{div})$ and the height was $\Delta Z = H/Z_{div}$. The subdomains could be referenced using integer indexes $i \in \{0, 1, 2, ..., R_{div} - 1\}$ and $j \in \{0, 1, 2, ..., Z_{div} - 1\}$ starting from the symmetry axis and the bottom of the tank. The subdomains were connected via two matrices of internal volumetric flows $\mathbf{Q_r} \in \mathbb{R}^{(Rdiv-1)\times Zdiv}$ and $\mathbf{Q_z} \in \mathbb{R}^{Rdiv\times(Zdiv-1)}$ in radial and axial direction respectively, defined as Equation 2 and 3:

$$Q_r^{i,j} = \int_0^{2\pi} \int_{j\Delta Z}^{(j+1)\Delta Z} (i+1)\Delta R * v_r(c) dz(c) d\theta(c),$$
$$c \in \mathbb{CELLS}, \frac{r(c)}{\Delta R} = i + 1, i \in [0, R_{div} - 1) \quad (2)$$

$$Q_z^{i,j} = \int_0^{2\pi} \int_{i\Delta R}^{(i+1)\Delta R} r(c) * v_z(c) dr(c) d\theta(c),$$
$$c \in \mathbb{CELLS}, \frac{z(c)}{\Delta Z} = j+1, j \in [0, Z_{div}-1) \quad (3)$$

Volume of each subdomain could be calculated as a matrix $\mathbf{V} \in \mathbb{R}^{R_{div} \times Z_{div}}$ via Equation 4, or could be alternatively approximated as a matrix of cylinder or annular cylinder volumes located at corresponding position in the tank. Volume averages of arbitrary scalar property, e.g. turbulent dissipation rate, could be calculated similarly as a matrix $\mathbf{E} \in \mathbb{R}^{R_{div} \times Z_{div}}$ via Equation 5:

$$V^{i,j} = \sum V(c), c \in \mathbb{CELLS}, i \leq \frac{r(c)}{\Delta R} \leq i+1, j \leq \frac{z(c)}{\Delta Z} \leq j+1 \quad (4)$$

$$E^{i,j} = \sum \epsilon(c) * V(c)/V^{i,j},$$
$$c \in \mathbb{CELLS}, i \leq \frac{r(c)}{\Delta R} \leq i+1, j \leq \frac{z(c)}{\Delta Z} \leq j+1 \quad (5)$$

The concept of "zones" were introduced when assembling and mapping the matrices of $\mathbf{Q_r}, \mathbf{Q_z}, \mathbf{V}, \mathbf{E}$... to the array of subdomains as shown in Equation 6:

$$zone(i,j) = \left\{ \begin{array}{c} r = (i+0.5)\Delta R \\ z = (j+0.5)\Delta Z \\ Q_L = \left\{ \begin{array}{cc} 0 & \text{if } i = 0 \\ Q_r^{i-1,j} & 1 \leq i \leq R_{div}-1 \end{array} \right. \\ Q_R = \left\{ \begin{array}{cc} 0 & \text{if } i = R_{div}-1 \\ Q_r^{i,j} & 0 \leq i < R_{div}-1 \end{array} \right. \\ Q_B = \left\{ \begin{array}{cc} 0 & \text{if } j = 0 \\ Q_z^{i,j-1} & 1 \leq j \leq Z_{div}-1 \end{array} \right. \\ Q_U = \left\{ \begin{array}{cc} 0 & \text{if } j = Z_{div}-1 \\ Q_z^{i,j} & 0 \leq j < Z_{div}-1 \end{array} \right. \\ V = V^{i,j} \\ \vdots \\ \overline{\epsilon} = E^{i,j} \\ \vdots \end{array} \right\} \quad (6)$$

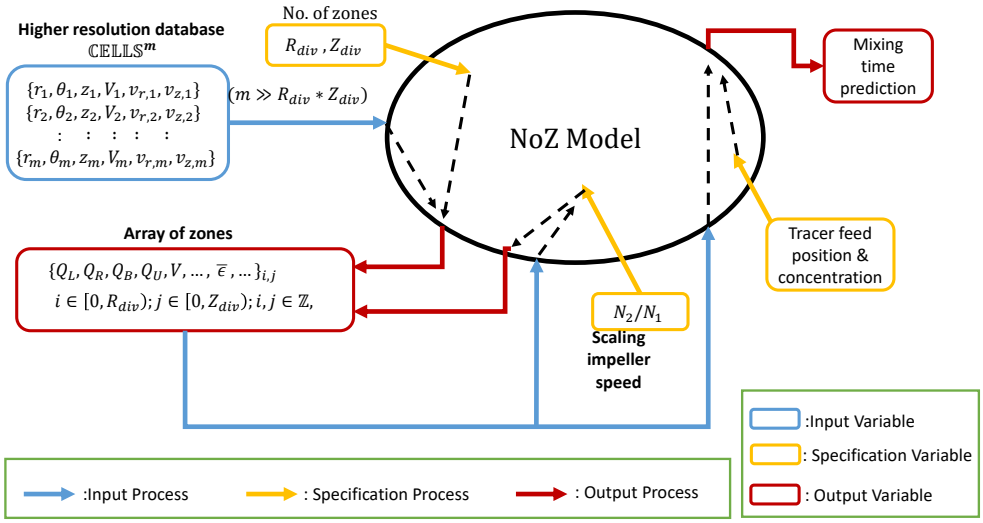

Figure 2: schematics of inputs, specifications and outputs of the NoZ model

The 2-D NoZ model defined the methodologies that approximate the flow field properties of every single cell $c \in \mathbb{CELLS}$ in each subdomain into mean properties of the corresponding zone so as to coarse-grain the higher resolution database while still being informative in characterisation of the geometry. The outputs of the NoZ model included volumetric flowrates between each zone and its neighbourhood zones Q_L, Q_R, Q_B, Q_U respectively as shown in Figure 1 which conserved the bulk flow patterns, volumes of the zones, and optionally volume-averages of scalar properties (such as transient concentrations or turbulent dissipation rates). With other optional specifications, additional outputs such as mixing time prediction could be obtained. An overall schematic of input, specifications and outputs was shown in Figure 2.

2.2. Bulk convective inter-zonal flowrates

Zones were connected via inter-zonal volumetric flowrates which were calculated via integrating orthogonal boundary fluxes over the boundary. In actual practice, rather than directly calculating the surface integral of the flux values over an unstructured CFD mesh, a simplified strategy of taking uniformly sampled points across the inter-zonal boundaries in both directions by interpolation was executed for better performance. Values at points on R-boundary surfaces were arithmetically averaged since the points

for interpolation were uniformly distributed, whilst points at Z-boundary surfaces were weighted by point radial coordinates, which could be derived from the expression of flow rate in pipe flows, as shown in Equation 7. In this work, each boundary surface was divided into 50 divisions in radial/axial direction and 720 divisions in the angular direction, which formed 36000 points for interpolation on each boundary. The bulk inter-zonal flowrates were then calculated by multiply the θ-ensembled average velocities $\bar{v}_{r,k}, \bar{v}_{z,k}$ with the boundary areas.

$$\begin{aligned} Q_r^{i,j} &\approx \frac{2\pi\Delta Z(i+1)\Delta R}{n} \sum_{k=1}^{n=50} \bar{v}_{r,k}\big|_{r=(i+1)\Delta R, z=(j+k/n)\Delta Z} \\ Q_z^{i,j} &\approx \frac{2\pi\Delta R}{n} \sum_{k=1}^{n=50} (r * \bar{v}_{z,k})\big|_{r=(i+k/n)\Delta R, z=(j+1)\Delta Z} \end{aligned} \tag{7}$$

2.3. Mass imbalance remediation

The established NoZ model introduced mass imbalances in some of the core zones, i.e. the total flowrates into the zone were unequal to the total flowrates out from the zone. The mass imbalance was mainly caused by two aspects: interpolation error and the "compression" from the 3-D CFD to the 2-D NoZ model. The interpolation amplified the mass flow rate deviation at the inter-zonal boundaries where there were steep velocity drops along the boundaries or across their adjacent zones in the 2-D NoZ model. The compression from 3-D to 2-D contributed to mass imbalance by the θ-averaging process when obtaining the flowrates, especially at the zones with periodic velocity changes in θ-direction, for example the impeller discharging zone and near-baffle zones. Mass imbalance of the NoZ model was then quantified and normalised by introducing the mass imbalance residual R_k and its normalised form $\|R_k\|$ of each zone k:

$$\begin{aligned} R_k &= \sum_{x}^{L,R,U,B} Q_{k,x} \\ \|R_k\| &= \frac{\mid R_k \mid}{\mathrm{Max}(\mid Q_{in,k} \mid, \mid Q_{out,k} \mid)} \end{aligned} \tag{8}$$

Where in Equation 8, the subscripts x represents for all neighbour zones of zone k (L, R, B, U represent for left, right, bottom, uppper neighbours respectively) ; $Q_{k,x}$ represents for the inter-zonal volumetric flowrate between

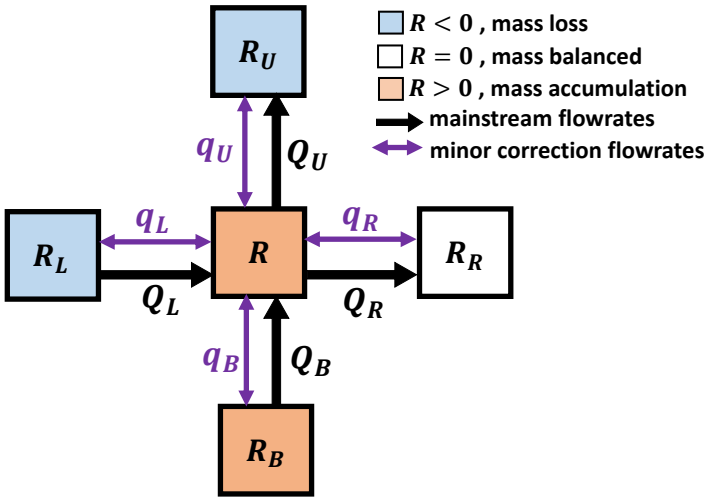

Figure 3: Schematic diagram of residual transport in remediation algorithm

zone k and zone x; $Q_{in,k}$, $Q_{out,k}$ represents for the sum of volumetric into and out from zone k.

To remedy the error brought by the presence of mass imbalance residual, an algorithm was developed to mitigate the value of mass imbalance residual. The basic methodology for the algorithm was to consider the mass imbalance residual as a typical passive-scalar transport problem. Zero residuals were attempted to be achieved via re-allocating local residuals of each zone and its neighbourhood zones while keeping the sum of the total absolute volumetric flow rate deviations (could be positive, negative or zero) all over the zonal map constant. This means only the distribution of the residuals in each zone and its neighbourhood zones were changed.

Figure 3 illustrated the preliminary definitions in the algorithm for each zone in the NoZ model. As stated previously, the absolute mass imbalance residuals of water (bulk fluid) in the concerned zone was denoted as R, whilst R_L, R_R, R_U, R_B represented for the absolute mass imbalance residual of water in the left, right, up and bottom neighbour zone respectively. Four additional inter-zonal flowrates (q_L, q_R, q_B, q_U) were defined as "minor correction flowrates" compared to the mainstream inter-zonal flowrates denoted as Q_L, Q_R, Q_B, Q_U, transporting the residuals among the central zone and its neighbourhood zones as R, R_L, R_R, R_U, R_B were assumed to be transported as general volume-based scalars.

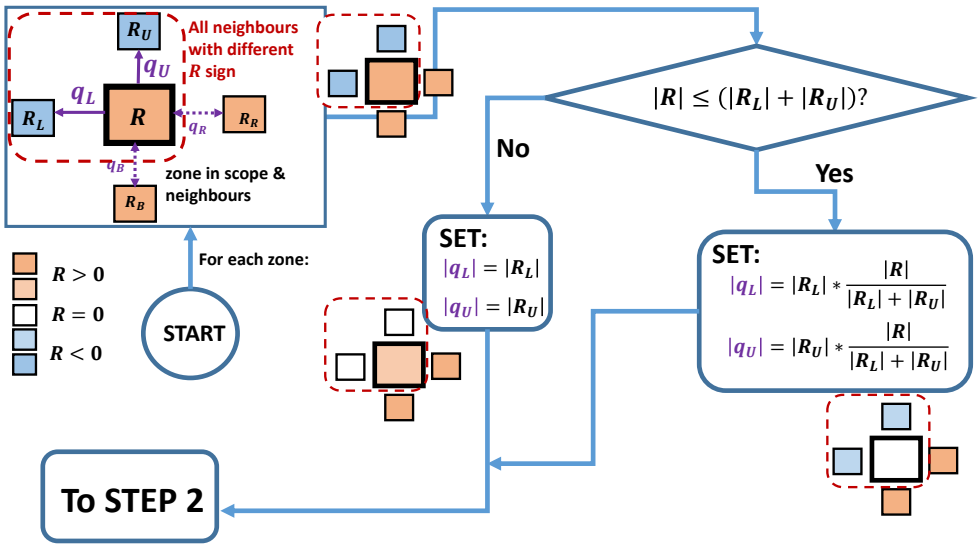

Figure 4: Schematic of STEP 1 in the remediation algorithm

The algorithm was run iteratively until the system was reduced to a desired tolerance of mass imbalance residual. Each iteration of the algorithm could be broken into two separate steps:

STEP 1: For each zone, find the neighbourhood residuals $R_k \in \{R_L, R_R, R_U, R_B\}$ that were of different sign with the zonal residual R, i.e. satisfying $(R * R_k) < 0$. Transport of residual between these zones could reduce the absolute value of mass imbalance since they were different in signs. This step created at least 1 zone that had zero residual as long as R_k satisfying $(R * R_k) < 0$ exists. The schematic diagram of this step was shown in Figure 4.

STEP 2: For each zone, the neighbourhood residuals $R_k \in \{R_L, R_R, R_U, R_B\}$ should all satisfy $(R * R_k \geq 0)$ after STEP 1. For $R_k \in \{R, R_L, R_R, R_U, R_B\}$ and volumes of the zones $V_i \in \{V, V_L, V_R, V_U, V_B\}$, residuals were further uniformly distributed based on zonal volume, i.e. set the inter-zonal q values so that $R_k/V_k = \sum_k R_k / \sum_k V_k$. This would re-fill the zones that with 0 residual with non-zero residuals of smaller absolute value while keeping the sum of the residuals constant as well.

After running STEP 1 and STEP 2, the new values of mass imbalance residual were calculated and compared to the desired tolerance. STEP 1 and STEP 2 were then iteratively executed until the desired tolerance was

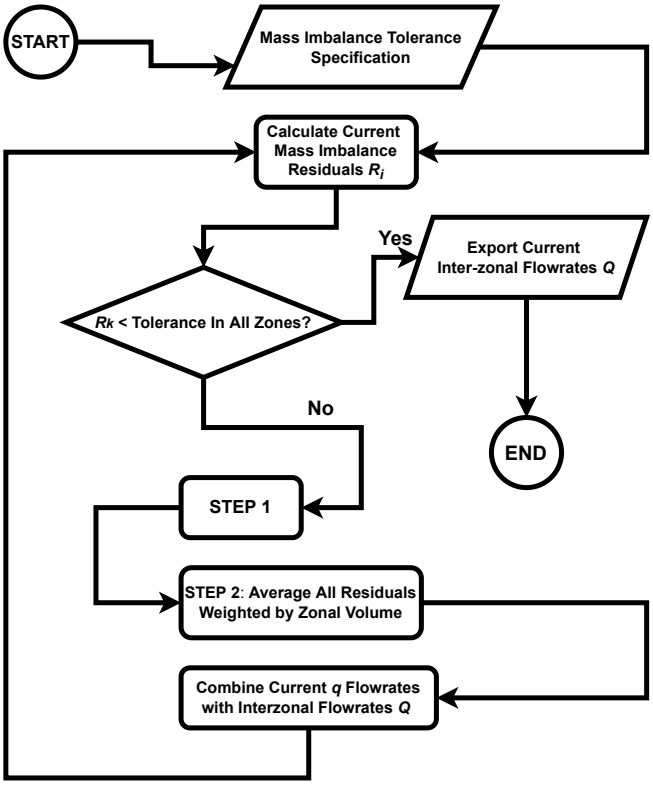

Figure 5: Overall flow chart of the remediation algorithm

reached, as shown in Figure 5.

2.4. Approximation for non-convective transports

The bulk convective inter-zonal flowrates in Section 2.2 were not considering all non-convective transport phenomena between neighbourhood zones, for instance turbulent diffusion and swirl flows with scales smaller than zone sizes. Quantitative descriptions on these effects were usually complicated, as they depended on specific turbulent models and involved secondary gradients on fluid properties, which further coupled with the main stream flows in smaller scales. In stirred vessels in the fully turbulent regime, an assumption could be made that the transport was dominated by convection, under

which an auxiliary inter-zonal flowrate Q_{diff} could be defined. Instead of solving differential equations on every inter-zonal boundaries for turbulent diffusion effect and secondary swirls, a uniformed value was assigned to Q_{diff} which represents the average transported flowrate by non-convective transport phenomena between every pair of connected zones. The value of the global constant Q_{diff} could be either specified zero when the studied stirred tank geometry was highly convection-dominant in aspect of the interested properties, or non-zero values with small magnitudes compared with largest bulk convective inter-zonal flowrates.

In this work, a quick approximation method of estimation the value of Q_{diff} was built based on general diffusive transport equation and averaging inter-zonal boundaries weighted by surface area, which could be estimated in Equation 9:

$$\frac{Q_{diff}}{\overline{\Gamma}} \approx \pi \Delta Z \frac{(M+1)(N+1)M + N\lambda^2(M+1)^2}{(M+1)N + (N+1)M} \tag{9}$$

In Equation 9 $M = R_{div} - 1$, $N = Z_{div} - 1$, $\lambda = \Delta R / \Delta Z$, $\overline{\Gamma}$ was the mean diffusion coefficient in the whole vessel. The RHS of Equation 9 was dependent on the scales and structure of the zone grid only whilst the denominator of LHS was dependent on the flow velocity field (from CFD) only. Hence, as long as one plausible value of $\overline{\Gamma}$ was estimated from known data from CFD, a Q_{diff} value to approximate non-convective transport in the NoZ model could be calculated at once.

2.5. Scaling of inter-zonal flowrates

In the fully turbulent regime, the bulk convective inter-zonal flowrates could be scaled linearly with impeller Reynolds number on exactly identical geometry and fluid. A NoZ model for a stirred tank geometry at an arbitrary impeller speed in fully turbulent regime could hence be generated by scaling the inter-zonal flowrates from an existing CFD-NoZ model of identical geometry and fluid by the factor of impeller speed ratios. In the fully turbulent regime, the value of Q_{diff} could be assumed to following same scaling method as the bulk inter-zonal flowrates as the bulk inter-zonal flowrates, since the non-convective inter-zonal transport were assumed to be dominated by turbulent diffusion. When turbulent Schmidt number remained identical, the diffusion coefficient could been scaled by a factor of mean turbulent viscosity $\overline{\nu_T}$ as shown in Equation 10, which resulted in the impeller speed ratio as well.

$$\frac{\overline{\nu_T}(N_2)}{\overline{\nu_T}(N_1)} \approx \frac{\overline{k}^2(N_2)/\overline{\epsilon}(N_2)}{\overline{k}^2(N_1)/\overline{\epsilon}(N_1)} \propto \frac{(N_2^2 * D^2)^2/(N_2^3 * D^2)}{(N_1^2 * D^2)^2/(N_1^3 * D^2)} = \frac{N_2}{N_1} \tag{10}$$

2.6. Mixing time prediction

Prediction of mixing time for reaching 95% homogeneity θ_{95} was based on the inter-zonal flowrates: the mixing process was assumed to be driven by convective inter-zonal flowrates and each zone was assumed to be homogeneous at each time step. At zero time t_0 a specified zone ("feed zone") was filled with inert tracer with a concentration of $C_{0,Feed}$ whilst other zones ("bulk zones") within the NoZ model contains concentration of $C_{0,Bulk}$ of tracer, which was often set as zero. Tracer concentrations of all zones at $t \to \infty$ were assumed to be perfectly mixed concentration, which could be obtained from the mass balance of tracer from the volume of feed zone V_{Feed} and volume of bulk zones V_{Bulk}:

$$C_\infty = \frac{C_{0,Feed} * V_{Feed} + C_{0,Bulk} * V_{Bulk}}{V_{Feed} + V_{Bulk}} \tag{11}$$

The velocities of the bulk fluid were assumed to be independent of tracer concentration, i.e. the addition of tracer had no impact on the dynamic properties of bulk fluid, for example, viscosity or density. The effects of mixing during the process of adding tracer into the feed zone were assumed to be negligible. The mixing process was simulated via solving differential mass balance equations iteratively. The initial specification of the time interval between time steps Δt was specified as 1% of θ_{95} obtained from literature correlation (Grenville and Nienow, 2004). The final time interval between time steps was found by a time step sensitivity test, i.e. time interval that no significant effects on mixing time prediction when further refining the time steps.The differential equation was derived based on the mass balance of the inert tracer. To balance the in-fluxes and out-fluxes of the zone, two operator functions for inter-zonal flow rates shown in Equation 12 were defined:

$$\delta_+ = \begin{cases} 1 & \text{flow in} \\ 0 & \text{flow out} \end{cases} \delta_- = \begin{cases} 0 & \text{flow in} \\ 1 & \text{flow out} \end{cases} \tag{12}$$

Then the differential mass balance, driven by convective mass transfer of inter-zonal fluxes and omitting diffusion of the tracer, could be expressed as Equation 13:

$$V_{i,j}\frac{dC_{i,j}}{dt} = \delta_+ Q_L C_{i-1,j} + \delta_+ Q_R C_{i+1,j} + \delta_+ Q_U C_{i,j+1} + \delta_+ Q_B C_{i-1,j} - C_{i,j}(\delta_- Q_L + \delta_- Q_R + \delta_- Q_U + \delta_- Q_B) \quad (13)$$

when specified a value of Q_{diff}, the above equations could be combined to the general control equation of each zone k as shown in Equation 14:

$$V_k\frac{dC_k}{dt} = \sum_{k,x}^{x=L,R,B,U} (\delta_+ Q_{k,x} + Q_{diff}) * C_x - (\delta_- Q_{k,x} + Q_{diff}) * C_k \quad (14)$$

Equation 14 could then be applied iteratively for each zone at each time step while monitoring the root mean square dimensionless variation shown in Equation 15:

$$ln(\sigma_{rms}) = \frac{1}{2} ln[\frac{1}{R_{div} * Z_{div}} \sum_{i}^{R_{div}-1} \sum_{j}^{Z_{div}-1} (C'_{i,j}(t) - 1)^2] \quad (15)$$

Where $C'_{i,j} = (C_{i,j} - C_0)/(C_\infty - C_0)$ was the dimensionless concentration (Brown et al., 2003) of $zone(i, j)$ in the system at a certain time whilst C_0 and C_∞ were concentrations of this zone at start time and after a sufficiently long time (which was often assumed as infinite time). The tank was assumed to achieve 95% homogeneity when the root mean square dimensionless variation satisfies $ln(\sigma_{rms}) <= 3.0$ (James et al., 2017), and the θ_{95} could then be found when plausible time step interval was specified.

3. Results and Discussion

The NoZ model was tested using two exemplar stirred tank geometries. The methodology was first applied to a Rushton impeller with diameter D=T/3 installed at a clearance of C=T/3 in a T=0.1m standard tank, with four B=T/10 baffles. The tank was filled with water and the impeller was rotating at a speed of N=2165 rpm which provided a fully turbulent impeller discharging flow at Re=40000. A preliminary CFD simulation using standard k-ϵ model (SKE) and multiple reference frames (MRF) method was solved and validated by experimental results (Coroneo et al., 2011; Aubin et al., 2004; Lee and Yianneskis, 1998) in literature, then the velocity fields

were interpolated and integrated at inter-zonal boundaries to assemble a NoZ model with (radial) 10*20 (axial) zones.

Mixing time was then solved using conservation of concentration, given a specified zone that was initialised as feed zone of high concentration of tracer (Rodgers et al., 2011). The dimensionless concentrations of all 200 zones and homogeneity of the vessel were then calculated (Brown et al., 2003; James et al., 2017) until a 95% homogeneity was achieved. The NoZ models of the same geometry at other impeller Reynolds numbers (from Re=20000 to Re=44000) in the fully turbulent regime were scaled from the Re=40000 NoZ model by linearly scaling the inter-zonal flowrates with impeller speed. In comparison, separate CFD simulations on the same geometry at different impeller Reynolds numbers were carried out to generate passive scalar transport mixing time predictions. The 95% mixing time (θ_{95}) was then compared with both CFD results and empirical correlations (Grenville and Nienow, 2004) within the Re range in the fully turbulent regime.

The procedure was then repeated again on a downflow pitched blade turbine (PBTD) with identical size, clearance and impeller speed in identical tank, except for quantified evaluation on performance of the remediation algorithm in Section 3.1.

3.1. Analysis of Remediation Algorithm

The remediation algorithm was realised by Python 3, setting the mass imbalance residual tolerance at 0.1%. One minor difference between the realisation in Python and the algorithm shown in Figure 5 was that instead of writing an external loop to compare the maximum current residual with the tolerance, the number of iterations were manually set to allow study of variation of the error with iteration. Each iteration took approximately 30 seconds to run including I/O streams on a PC. Figure 6 showed that the mass imbalance residual was reduced rapidly in first 4 iterations, whilst the remaining minor residual took at least 5 more iterations to be reduced down below the tolerance. This was because the more iterations were run, the correction flowrates q were lower in magnitude and hence the transportation of the residuals was slower.

The comparison between the inter-zonal flowrates before and after remediation was shown in Figure 7. The algorithm managed to preserve most flow patterns and key inter-zonal flowrates (i.e. impeller discharging flows and re-circulations) while reducing the mass imbalance flowrate, except for altering several trivial inter-zonal flow with extremely low flow rates near the

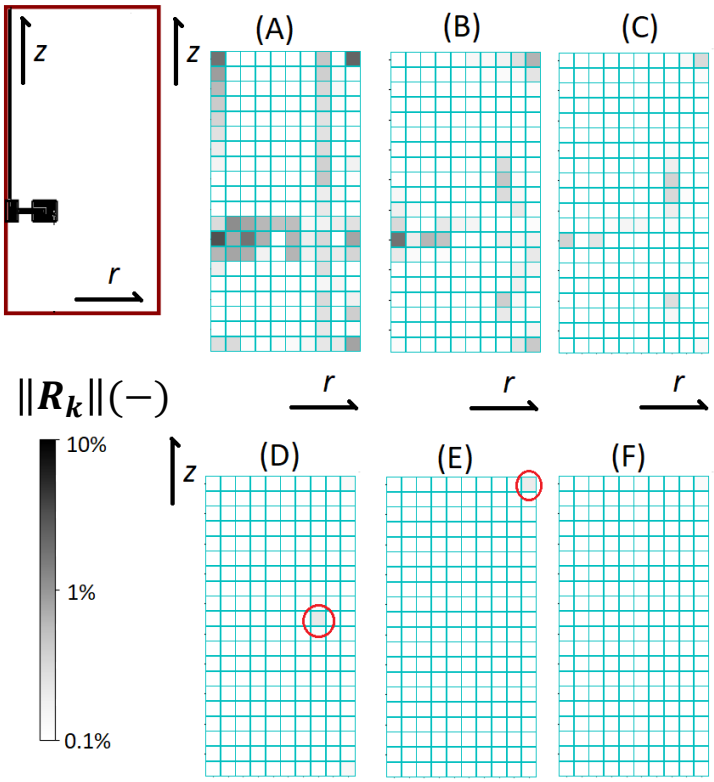

Figure 6: Normalised mass imbalance residuals of (A) before remediation, (B) after 1 iteration, (C) after 2 iterations, (D) after 4 iterations, (E) after 8 iterations, and (F) after 16 iterations in single Rushton tank at Re=40000

impeller hub and shaft. The percentage difference in mixing time predicted using method mentioned in Section 3.2 between using NoZ model before remediation and after 16 remediation iterations was 0.7%, which showed that the effect of remediation iterations executed on mixing time prediction was negligible.

3.2. Mixing Time Estimation of exemplar geometries

The red dash-and-dot lines in Figure 8 were ±20% deviation from the laboratory correlation (Grenville and Nienow, 2004) using CFD power numbers, ranging for 95% confidence of mixing time prediction. The laboratory correlation (Grenville and Nienow, 2004) was based on the theory that in turbulent regime the dimensionless mixing time is a function of power number and impeller / tank size ratios but independent of impeller type on selected

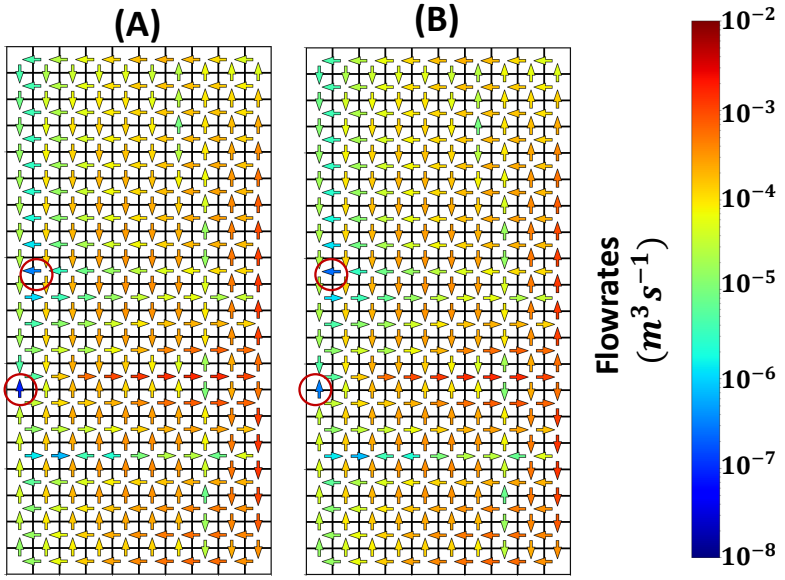

Figure 7: Comparison of inter-zonal flowrate in single Rushton tank at Re=40000 of (A) before mass-imbalance remediation and (B) after 16 iterations of remediation

range of impeller types, which had been supported by literature laboratory observations (Nienow, 1997; Strand, 2017). Figure 8 showed that mixing time predicted by the NoZ models were consistent with that predicted by the CFD passive scalar transport methods at all Reynolds number ranging from 20000 to 40000. Mixing time predicted via NoZ model also decreased inverse proportionally with increasing impeller speed, which were consistent with Grenville and Nienow (2004) as well.

Figure 9 showed the sensitivity of mixing time predicted via NoZ model on specification of Q_{diff} values. The top abscissa represented for the ratio of specified Q_{diff} values to the maximum magnitude of convective inter-zonal flowrates in the two geometries respectively. As a reference, the green lines represented for zero-flowrate NoZ model mixing time estimations, i.e. zero inter-zonal flowrates among every zones and mixing were only driven by the specified Q_{diff} flowrates. The green lines indicated that in both tested geometries, when the value of Q_{diff} were at the same order of magnitude as calculated values using Equation 9, mixing time driven by Q_{diff} only was around one order of magnitude higher than that predicted by convective-driven NoZ model; when the Q_{diff} increased above approx. 10 times of calculated value using Equation 9 mixing started to be dominated by Q_{diff} rather than the

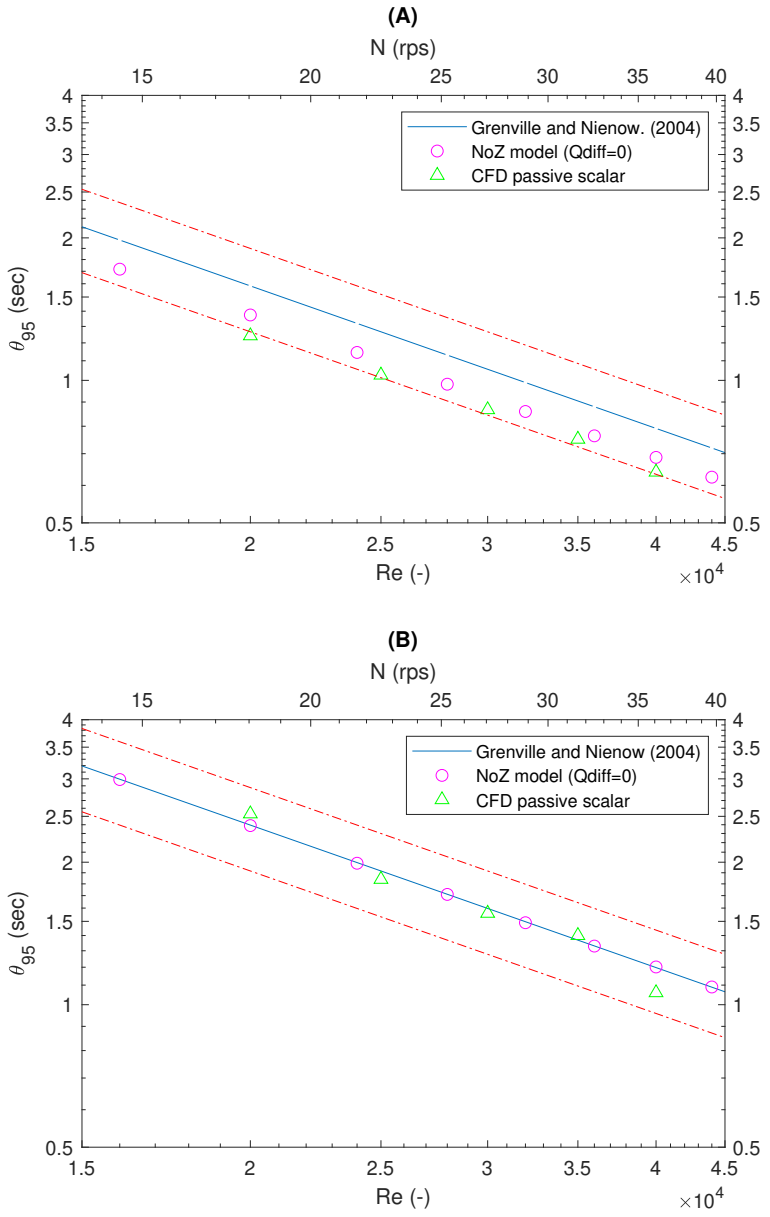

Figure 8: Mixing time predicted on (A)single Rushton tank and (B)single PBTD tank. Red dash-and-dot lines represents for ± 20% deviation from blue line.

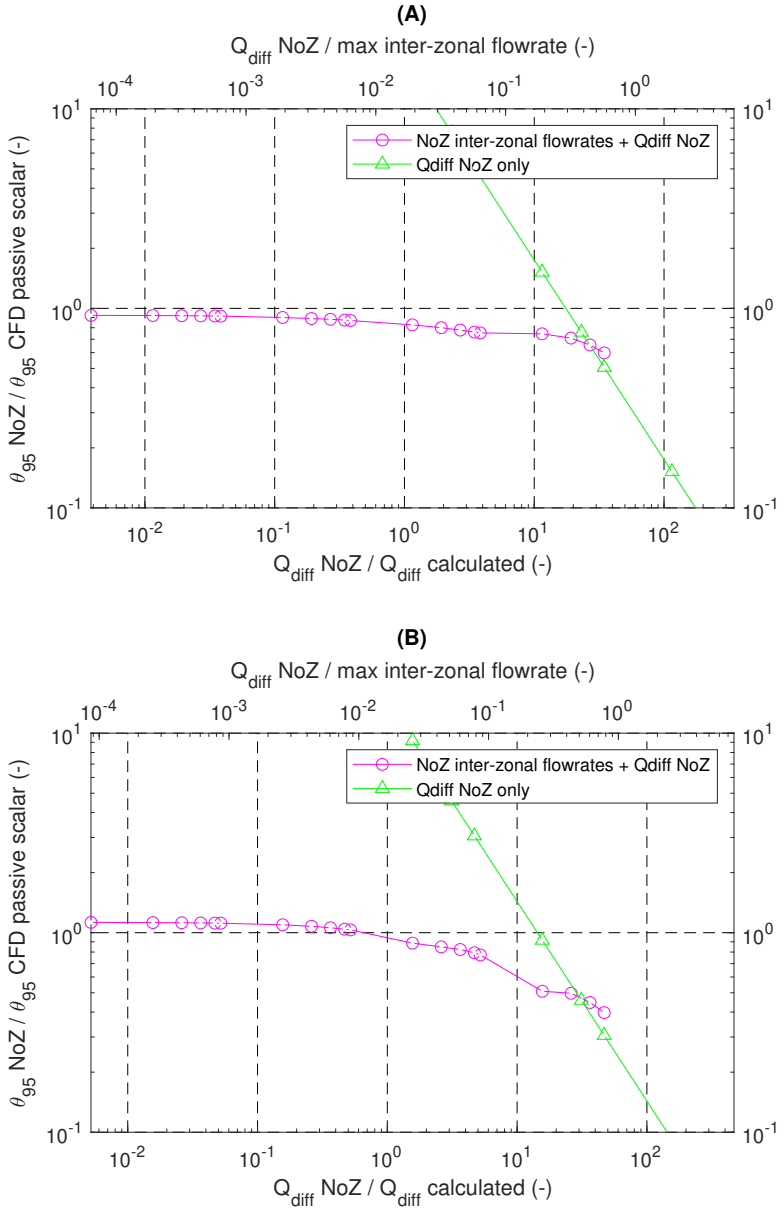

Figure 9: Mixing time sensitivity on Q_{diff} values (A)single Rushton tank and (B)single PBTD tank, Re=40000, normalised by Q_{diff} calculated using Equation 9 or maximum inter-zonal flowrate in Noz model with $Q_{diff} = 0$

Table 1: Sensitivity of dimensionless mixing time $N\theta_{95}$ (-) on number of zones (R_{div}*Z_{div})

Geometry	single Rushton Tank	single PBTD Tank
NoZ (8*15)	24	46
NoZ (10*20)	25	43
NoZ (12*23)	31	45
Grenville and Nienow (2004)	27±5.5	43±8.6

convective-inter-zonal flowrates. The red curves showed that the specifications of Q_{diff} values one order of magnitude lower than calculated value using Equation 9 value had trivial impact on mixing time predicted. Combining both curves, the specification of Q_{diff} values using Equation 9 were consistent to the assumption of convective-dominated NoZ model and were able to contribute minor mixing enhancements caused by diffusive transports.

Table 1 showed the sensitivity of number of zones on predicted mixing time. Table 1 showed that effect of number of zones on mixing time predicted in standard PBTD tank was very small, and all lied within the experimental range of mixing time (Grenville and Nienow, 2004). For the standard Rushton case, the 12*23 zones NoZ model predicted a slightly higher mixing time. One possible reason for this over-prediction was that the impeller discharging flows of Rushton impellers were strongly radial, where transport in axial direction along discharging flows was de facto dominated by local turbulent diffusion; increasing number of axial boundaries could then increase the number of boundaries where the convection-dominant assumption may not be satisfied. However, as it still lied within the experimental range of mixing time, Table 1 suggested a weak grid size sensitivity of the NoZ model at least in mixing time prediction when number of zones were in appropriate range.

3.3. Turbulent dissipation rates profiles

Turbulent dissipation rates in the two exemplar geometries at Re=40000 were exported from CFD respectively together with CFD cell volumes. In each of the zones in the two studied NoZ models (with 10*20 zones), the zonal average turbulent dissipation rate was calculated as the volume-weighted average turbulent dissipation rate of all CFD cells locating within the zone before normalised by the volume averaged turbulent disspation rates of the entire tanks, which in laboratory studies could be more easily estimated by

measuring power consumption. Figure 10 showed the comparison between generated 2-D NoZ patterns of turbulent dissipation rates and snapshots of two extreme positions away from the baffles in CFD (between two adjacent impeller tips and aligning at the impeller tips) in two exemplar geometries respectively. In addition, Figure 10(C) and Figure 10(E) also showed the turbulent dissipation rate just behind baffles at the near wall regions. The turbulent dissipation rate patterns in NoZ models of both geometries tightened the extremely low and high ends of local dissipation rates while conserving their decaying propagation along impeller discharging flows. The NoZ models of neither geometries had flow volume where the zonal dissipation rate was higher than $100\bar{\epsilon}$.

The generated coarse-grained local turbulent dissipation rate profiles and distributions could then be used as a guideline for local droplet breakups in emulsification, as a group of droplet size distribution metrics could be correlated with local turbulent dissipation rates (Vankova et al., 2007), or alternatively as an input for pupulation balance model for system with low volume fraction of the dispersed phase (Naeeni and Pakzad, 2019; Liu et al., 2016). Figure 11 showed that in both exemplar geometries, fluid volume with normalised turbulent dissipation rates outside the range $[0.01, 100]$ in CFD were negligible in both CFD and NoZ model, indicating the truncation in NoZ models of extreme low and high ends from CFD would have limited impact when predicting of local droplet size distributions. Figure 11 also showed that the NoZ model conserved the distributions of local dissipation rates from CFD over the entire volume domain of the two exemplar stirred tanks. The normalised turbulent dissipation profile could be also used when scaling the impeller Reynolds number, as the global volume-averaged turbulent dissipation rate could be estimated via power input per unit mass in fully turbulent regime, which could be scaled by the factor of $\rho N^3 D^5$ for the same type of impeller (Hemrajani and Tatterson, 2003).

3.4. Time consumption

The most time consuming step of the entire workflow was the generation of inter-zonal flowrates compared to mass imbalance remediation and mixing time estimation. This was mainly because the interpolation of 3-D converged CFD data were realised using Python 3 SciPy library function interpolate.griddata(), the time consumption of which would be considerably long when number of known values were with order of magnitude of million rows. Putting the entire CFD data all into RAM was also challenging

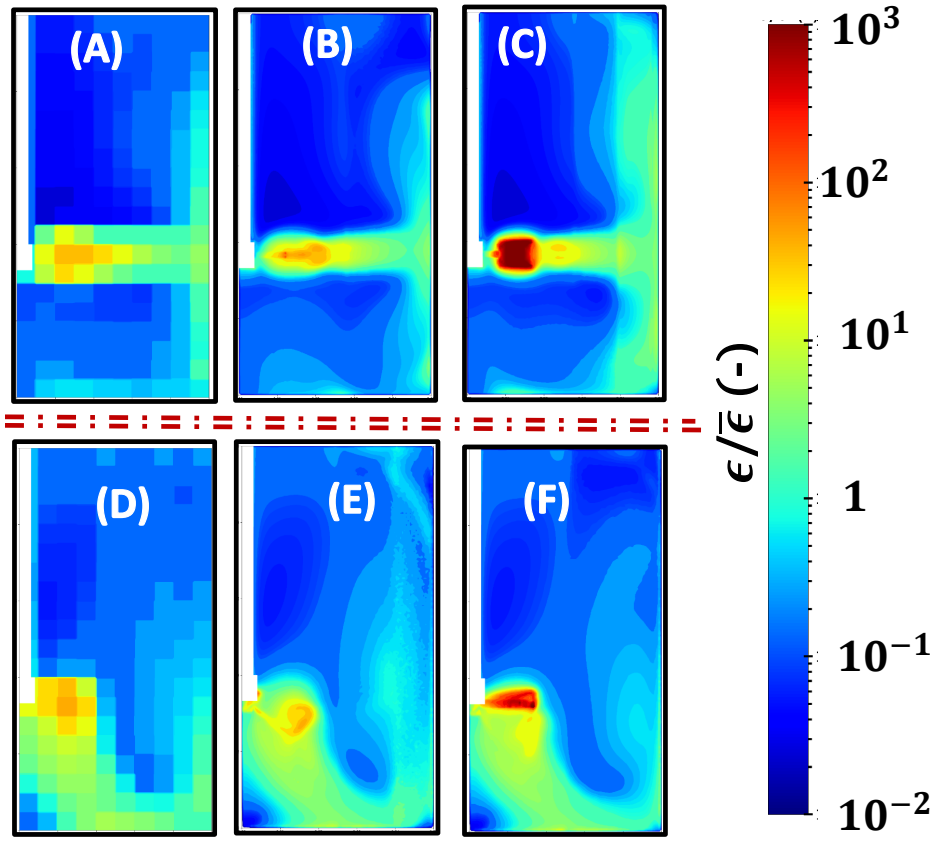

Figure 10: Turbulent dissipation rate profiles in Re=40000 single Rushton ((A) to (C)) and single PBTD ((D) to (F)) tanks: (A)(D) NoZ model, (B)(E) CFD, between impeller tips and (C)(F) CFD, at impeller tips, normalised by CFD global volume-averaged turbulent dissipation rates

especially when the process was executed on a PC with more limited RAM storage. A more conservative strategy which interpolate one boundary a time was hence adapted by reading the CFD data multiple times as a compromise, so that the process could be executed on PCs with more common specifications. The average serial process time for generating convective inter-zonal flowrates was approx. 2-3 seconds per boundary, excluding time consumed for reading CFD data in comma-separated values (.csv) file which was approx 4 seconds per boundary.

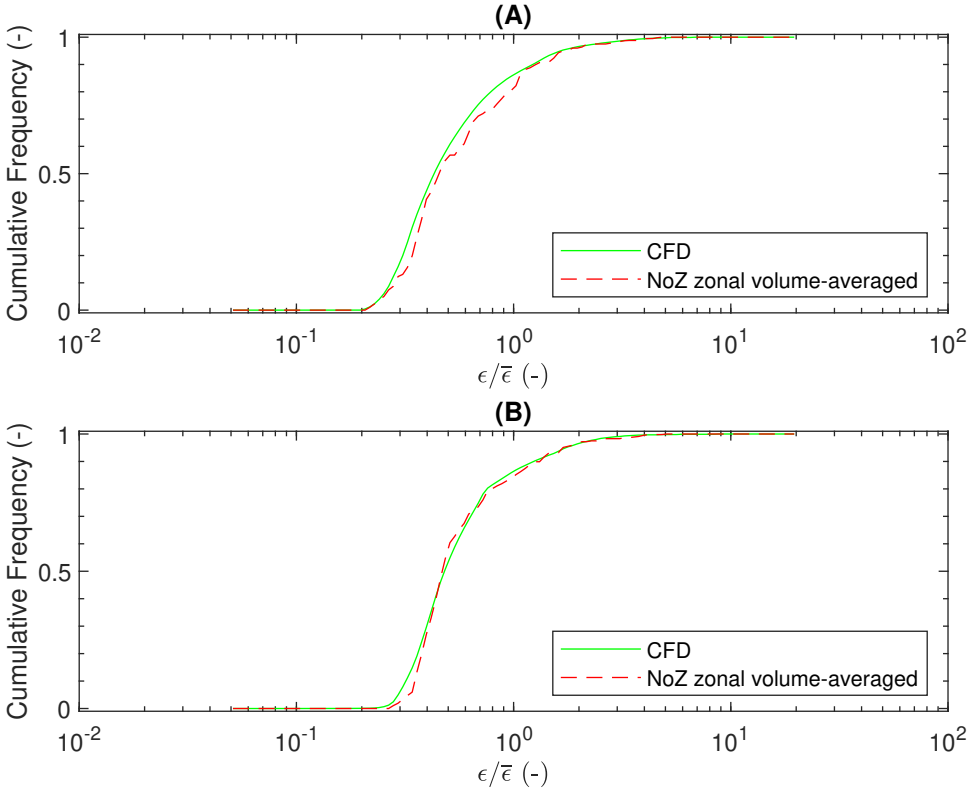

Figure 11: Volume-weighted cumulative frequencies of turbulent dissipation rates in (A) single Rushton tank and (B) single PBTD tank, normalised by global volume-averaged turbulent dissipation rates ($\overline{\epsilon}$), Re=40000

3.5. Limitation

As the 2-D NoZ model was based on the assumption that inter-zonal transport was dominated by convection, critical judgements need to be made on the mixing time predicted by 2-D NoZ model under special flow profiles. It had been observed that when zone boundaries were aligned with the symmetry plane of discharging flows near the impeller discharging region (for instance, in the NoZ model of single Rushton standard tank, when zone boundaries aligned with the Rushton disc along radial direction downstream the discharging flow, dividing the flow symmetrically), mixing time predicted were significantly longer than the zone grids that were not, despite specifying non-zero Q_{diff} values using Equation 9 would mitigate the over-prediction.

This was probably because the NoZ method were not able to preserve local turbulent diffusion processes, whilst transport across the symmetry plane of discharging flows were in fact dominated by local turbulent diffusion. One plausible solution to this over-prediction was to avoid this alignment between zone boundaries with symmetry plane by altering number of zones slightly in corresponding directions, as the NoZ model was not requiring a strictly unity aspect ratio between the width and height of the zone.

In addition to the limitation mentioned above, the obtained estimations of any stirred vessel systems should be handled critically if the major assumptions of the methodology established in this work were not satisfied. For instance, the 2-D NoZ topology restricted the validity of any transport phenomena which are dominated by tangential flows, where instead a 3-D NoZ model involving azimuthal topology of the vessels could provide more plausible estimations. Applications to multiphase flows with high volume fraction of the dispersed phase but starting from the turbulent energy metrics from the volume averaged single phase CFD data should also be avoided, as the assumptions of constant density and homogeneous zone were not satisfied in these situations.

4. Conclusion & Suggested Future Works

The established 2-D NoZ model managed to generate two-dimensional bulk inter-zonal flowrates profile while preserving the mainstream flow patterns from three-dimensional input database. The mass imbalance remediation algorithm managed to mitigate the mass imbalance in the bulk inter-zonal flowrate lists without introducing significant deviations from actual flow patterns. The prediction of mixing time based on the 2-D NoZ model was consistent with correlated values from literature in standard tank case with both single Rushton and single D=T/3 PBTD impellers. The optional Q_{diff} method approximated the minor interactive transports between adjacent zones subjected to the assumption of convection domination, the mixing time sensitivity on which proved the quantified value of Q_{diff} were plausible on both exemplar geometries.

The methodology introduced in this work is a potential methodology that could be applied to further decisive scenarios. The main advantage of the 2-D NoZ methodology introduced in this work relied in its nature of the much lower computational space complexity compared to the scale of a typical CFD mesh, which would be ideal for potential further application to

coupled modelling problems where mainstream flow patterns were important whilst the total computational time complexity was strongly sensitive to space sensitivity (i.e. number of zones or mesh cells), for instance when local mechanisms involved strong interactions with global metrics.

One following future work that industries with various types of mixer geometries have been interested in is to weaken the dependence of generating NoZ model on exact preliminary CFD file. As these businesses are usually dealing with intense mixer geometry selections from a large range of candidates designs, a preliminary CFD and its conversion to 2-D NoZ model for every candidate geometry design will accumulate to a considerable time consumption before the due that decision are expected to be made. Hence, the next future work is to figure out a rapid method to generate the 2-D NoZ model with arbitrary impeller (and combination of impellers) and tank geometries starting from limited number of 2-D NoZ models obtained from preliminary CFD. This will enable an acceleration in designing processes by filtering out impossible geometrical designs quickly.

5. Acknowledgements

The authors acknowledge the financial and all other supports from the EPSRC and Unilever for the industrial case award and the EPSRC Project: Centre in Advanced Fluid Engineering for Digital Manufacturing (EP/R00 482X/1).

References

Aubin, J., Fletcher, D.F., Xuereb, C., 2004. Modeling turbulent flow in stirred tanks with CFD: The influence of the modeling approach, turbulence model and numerical scheme. Experimental Thermal and Fluid Science 28, 431–445. doi:10.1016/j.expthermflusci.2003.04.001.

Bakker, A., Myers, K.J., Ward, R.W., Lee, C.K., 1996. The laminar and turbulent flow pattern of a pitched blade turbine. Chemical Engineering Research and Design 74, 485–491.

Bezzo, F., Macchietto, S., 2004. A general methodology for hybrid multizonal/CFD models: Part II. Automatic zoning. Computers and Chemical Engineering 28, 513–525. doi:10.1016/j.compchemeng.2003.08.010. part2.

Bezzo, F., Macchietto, S., Pantelides, C.C., 2003. General hybrid multizonal/CFD approach for bioreactor modeling. AIChE Journal 49, 2133–2148. doi:10.1002/aic.690490821.

Bezzo, F., Macchietto, S., Pantelides, C.C., 2004. A general methodology for hybrid multizonal/CFD models: Part I. Theoretical framework. Computers and Chemical Engineering 28, 501–511. doi:10.1016/j.compchemeng.2003.08.004. part1.

Brown, D.A.R., Jones, P.N., Middleton, J.C., Papadopoulos, G., Arik, E.B., 2003. Experimental Methods, in: Handbook of Industrial Mixing. John Wiley & Sons, pp. 145–256. URL: https://doi.org/10.1002/0471451452.ch4, doi:10.1002/0471451452.ch4. series Title: Wiley Online Books.

Chen, C., Guan, X., Ren, Y., Yang, N., Li, J., Kunkelmann, C., Schreiner, E., Holtze, C., Mülheims, K., Sachweh, B., 2019. Mesoscale modeling of emulsification in rotor-stator devices: Part I: A population balance model based on EMMS concept. Chemical Engineering Science 193, 171–183. URL: https://www.sciencedirect.com/science/article/pii/S0009250918306286, doi:10.1016/j.ces.2018.08.048.

Coroneo, M., Montante, G., Paglianti, A., Magelli, F., 2011. CFD prediction of fluid flow and mixing in stirred tanks: Numerical issues

about the RANS simulations. Computers and Chemical Engineering 35, 1959–1968. URL: http://dx.doi.org/10.1016/j.compchemeng.2010.12.007, doi:10.1016/j.compchemeng.2010.12.007. publisher: Elsevier Ltd.

Grenville, R.K., Nienow, A.W., 2004. Blending of Miscible Liquids. John Wiley & Sons. doi:10.1002/0471451452.ch9. publication Title: Handbook of Industrial Mixing.

Haag, J., Gentric, C., Lemaitre, C., Leclerc, J.P., 2018. Modelling of Chemical Reactors: From Systemic Approach to Compartmental Modelling. International Journal of Chemical Reactor Engineering 16, 1–22. doi:10.1515/ijcre-2017-0172.

Han, L., Liu, Y., Luo, H., 2007. Numerical Simulation of Gas Holdup Distribution in a Standard Rushton Stirred Tank Using Discrete Particle Method. Chinese Journal of Chemical Engineering 15, 808–813. doi:10.1016/s1004-9541(08)60007-5.

Hemrajani, R.R., Tatterson, G.B., 2003. Mechanically Stirred Vessels, in: Handbook of Industrial Mixing. John Wiley & Sons, pp. 345–390. URL: https://doi.org/10.1002/0471451452.ch6, doi:10.1002/0471451452.ch6. series Title: Wiley Online Books.

Hsu, T.J., Mou, C.Y., Lee, D.J., 1994. Effects of Macromixing on the oregonator model of the belousov - zhabotinsky reaction in a stirred reactor. Chemical Engineering Science 49, 5291–5305. doi:10.1016/0009-2509(94)00278-9.

Håkansson, A., Chaudhry, Z., Innings, F., 2016. Model emulsions to study the mechanism of industrial mayonnaise emulsification. Food and Bioproducts Processing 98, 189–195. URL: https://www.sciencedirect.com/science/article/pii/S0960308516000237, doi:10.1016/j.fbp.2016.01.011.

James, J., Cooke, M., Kowalski, A., Rodgers, T.L., 2017. Scale-up of batch rotor-stator mixers. Part 2—Mixing and emulsification. Chemical Engineering Research and Design 124, 321–329. URL: http://dx.doi.org/10.1016/j.cherd.2017.06.032, doi:10.1016/j.cherd.2017.06.032. publisher: Institution of Chemical Engineers.

Janssen, J.J., Hoogland, H., 2014. Modelling strategies for emulsification in industrial practice. The Canadian Journal of Chemical Engineering 92, 198–202. URL: https://onlinelibrary.wiley.com/doi/abs/10.1002/cjce.21942, doi:10.1002/cjce.21942. _eprint: https://onlinelibrary.wiley.com/doi/pdf/10.1002/cjce.21942.

Jaworski, Z., Dyster, K.N., Nienow, A.W., 2001. The effect of size, location and pumping direction of pitched blade turbine impellers on flow patterns: LDA measurements and CFD predictions. Chemical Engineering Research and Design 79, 887–894. doi:10.1205/02638760152721406.

Jourdan, N., Neveux, T., Potier, O., Kanniche, M., Wicks, J., Nopens, I., Rehman, U., Le Moullec, Y., 2019. Compartmental Modelling in chemical engineering: A critical review. Chemical Engineering Science 210, 115196. URL: https://doi.org/10.1016/j.ces.2019.115196, doi:10.1016/j.ces.2019.115196. publisher: Elsevier Ltd.

Kagoshima, M., Mann, R., 2006. Development of a networks-of-zones fluid mixing model for an unbaffled stirred vessel used for precipitation. Chemical Engineering Science 61, 2852–2863. doi:10.1016/j.ces.2005.11.054.

Komrakova, A.E., Liu, Z., Machado, M.B., Kresta, S.M., 2017. Development of a zone flow model for the confined impeller stirred tank (CIST) based on mean velocity and turbulence measurements. Chemical Engineering Research and Design 125, 511–522. URL: http://dx.doi.org/10.1016/j.cherd.2017.07.025, doi:10.1016/j.cherd.2017.07.025. publisher: Institution of Chemical Engineers.

Kresta, S.M., Wood, P.E., 1993. The flow field produced by a pitched blade turbine: Characterization of the turbulence and estimation of the dissipation rate. Chemical Engineering Science 48, 1761–1774. doi:10.1016/0009-2509(93)80346-R.

Le Moullec, Y., Gentric, C., Potier, O., Leclerc, J.P., 2010. Comparison of systemic, compartmental and CFD modelling approaches: Application to the simulation of a biological reactor of wastewater treatment. Chemical Engineering Science 65, 343–350. URL: https://www.sciencedirect.com/science/article/pii/S000925090900431X, doi:10.1016/j.ces.2009.06.035.

Lebaz, N., Sheibat-Othman, N., 2019. A population balance model for the prediction of breakage of emulsion droplets in SMX+ static mixers. Chemical Engineering Journal 361, 625–634. URL: https://www.sciencedirect.com/science/article/pii/S1385894718325762, doi:10.1016/j.cej.2018.12.090.

Lee, K.C., Yianneskis, M., 1998. Turbulence Properties of the Impeller Stream of a Rushton Turbine. AIChE Journal 44, 13–24. doi:10.1002/aic.690440104.

Liu, N., Wang, W., Han, J., Zhang, M., Angeli, P., Wu, C., Gong, J., 2016. A PIV investigation of the effect of disperse phase fraction on the turbulence characteristics of liquid–liquid mixing in a stirred tank. Chemical Engineering Science 152, 528–546. URL: https://www.sciencedirect.com/science/article/pii/S0009250916303360, doi:10.1016/j.ces.2016.06.040.

Massmann, T., Kocks, C., Parakenings, L., Weber, B., Jupke, A., 2020. Two-Dimensional CFD based compartment modeling for dynamic simulation of semi-batch crystallization processes in stirred tank reactors. Computers & Chemical Engineering 140, 106933. URL: https://www.sciencedirect.com/science/article/pii/S0098135420301162, doi:10.1016/j.compchemeng.2020.106933.

Naeeni, S.K., Pakzad, L., 2019. Droplet size distribution and mixing hydrodynamics in a liquid–liquid stirred tank by CFD modeling. International Journal of Multiphase Flow 120, 103100. URL: https://www.sciencedirect.com/science/article/pii/S0301932218308541, doi:10.1016/j.ijmultiphaseflow.2019.103100.

Nauha, E.K., Kálal, Z., Ali, J.M., Alopaeus, V., 2018. Compartmental modeling of large stirred tank bioreactors with high gas volume fractions. Chemical Engineering Journal 334, 2319–2334. URL: https://www.sciencedirect.com/science/article/pii/S1385894717321046, doi:10.1016/j.cej.2017.11.182.

Nienow, A.W., 1997. On impeller circulation and mixing effectiveness in the turbulent flow regime. Chemical Engineering Science 52, 2557–2565. URL: https://www.sciencedirect.com/science/article/pii/S0009250997000729, doi:10.1016/S0009-2509(97)00072-9.

Nørregaard, A., Bach, C., Krühne, U., Borgbjerg, U., Gernaey, K.V., 2019. Hypothesis-driven compartment model for stirred bioreactors utilizing computational fluid dynamics and multiple pH sensors. Chemical Engineering Journal 356, 161–169. URL: https://www.sciencedirect.com/science/article/pii/S1385894718316711, doi:10.1016/j.cej.2018.08.191.

Pigou, M., Morchain, J., 2015. Investigating the interactions between physical and biological heterogeneities in bioreactors using compartment, population balance and metabolic models. Chemical Engineering Science 126, 267–282. URL: https://www.sciencedirect.com/science/article/pii/S0009250914006897, doi:10.1016/j.ces.2014.11.035.

Rodgers, T.L., Siperstein, F.R., Mann, R., York, T.A., Kowalski, A., 2011. Comparison of a networks-of-zones fluid mixing model for a baffled stirred vessel with three-dimensional electrical resistance tomography. Measurement Science and Technology 22. doi:10.1088/0957-0233/22/10/104014.

Strand, A., 2017. Investigation of Blend Time for Turbulent Newtonian Fluids in Stirred Tanks. Master's thesis. Rochester Institute of Technology. New York. URL: https://scholarworks.rit.edu/theses/9686.

Tajsoleiman, T., Spann, R., Bach, C., Gernaey, K.V., Huusom, J.K., Krühne, U., 2019. A CFD based automatic method for compartment model development. Computers & Chemical Engineering 123, 236–245. URL: https://www.sciencedirect.com/science/article/pii/S0098135418308950, doi:10.1016/j.compchemeng.2018.12.015.

Vankova, N., Tcholakova, S., Denkov, N.D., Vulchev, V.D., Danner, T., 2007. Emulsification in turbulent flow: 2. Breakage rate constants. Journal of Colloid and Interface Science 313, 612–629. URL: https://www.sciencedirect.com/science/article/pii/S0021979707005413, doi:10.1016/j.jcis.2007.04.064.

Vlaev, D., Mann, R., Lossev, V., Vlaev, S.D., Zahradnik, J., Seichter, P., 2000. Macro-mixing and streptomyces fradiae modelling oxygen and nutrient segregation in an industrial bioreactor. Chemical Engineering Research and Design 78, 354–362. doi:10.1205/026387600527473.